Niedzwiedzki, D. M., Gardiner, A. T., Blankenship, R. E. and Cogdell, R. J. (2018) Energy transfer in purple bacterial photosynthetic units from cells grown in various light intensities. *Photosynthesis Research*, (doi:10.1007/s11120-018-0512-1)

This is the author's final accepted version.

There may be differences between this version and the published version. You are advised to consult the publisher's version if you wish to cite from it.

http://eprints.gla.ac.uk/162326/

Deposited on: 13 June 2018

Enlighten – Research publications by members of the University of Glasgow
http://eprints.gla.ac.uk

Energy Transfer in Purple Bacterial Photosynthetic Units from Cells Grown in Various Light Intensities

Dariusz M. Niedzwiedzki[1*], Alastair T. Gardiner[2], Robert E. Blankenship[1,3,4] and Richard J. Cogdell[2]

[1]*Photosynthetic Antenna Research Center, University in St Louis, MO 63130, USA*

[2]*Biomedical Research Building, Institute of Biomedical and Life Sciences, University of Glasgow, Glasgow, UK*

[3]*Departments of Biology and* [4]*Chemistry Washington University in St Louis, MO 63130, USA*

*Corresponding author: Dariusz M. Niedzwiedzki; Photosynthetic Antenna Research Center, Washington University in St. Louis, St. Louis, MO 63130, Campus Box 1138, USA. Tel.: +1 (314) 935-8483; fax +1 (314) 935-4925.

Abbreviations

AFM – atomic force microscopy

BChl – bacteriochlorophyll

DDM – *n* -Dodecyl-β-D-maltoside

FWHM – full width at half maximum

HL – high light

ICM – intra-cytoplasmic membrane

IRF – instrument response function

LDAO – N,N-Dimethyldodecylamine N-oxide

LH1-RC – light harvesting 1-reaction center

LH2 – light-harvesting 2

LL – low light

PMMA – poly(methyl methacrylate)

PSU – photosynthetic unit

RT – room temperature

TA – transient absorption

WT – wild type

Keywords: purple bacteria, light harvesting complex, transient absorption, energy transfer, intra-cytoplasmic membrane

Abstract

Three photosynthetic membranes called intra-cytoplasmic membranes (ICMs) from wild-type and the Δ*puc*BA$_{abce}$ mutant of the purple phototrophic bacterium *Rps. palustris* were investigated using optical spectroscopy. The ICMs contain identical light harvesting complex 1-reaction center (LH1-RC) but have various spectral forms of light-harvesting complex 2 (LH2). Spectroscopic studies involving steady-state absorption, fluorescence and femtosecond time-resolved absorption at room temperature and at 77 K focused on inter-protein excitation energy transfer. The studies investigated how energy transfer is affected by altered spectral features of the LH2 complexes as those develop under growth at different light conditions. The study shows that LH1→LH2 excitation energy transfer is strongly affected if the LH2 complex alters its spectroscopic signature. The LH1→LH2 excitation energy transfer rate modelled with the Förster mechanism and kinetic simulations of transient absorption of the ICMs demonstrated that the transfer rate will be 2-3 times larger for ICMs accumulating LH2 complexes with the classical B800-850 spectral signature (grown in high light) compared to the ICMs from the same strain grown in low light. For the ICMs from the Δ*puc*BA$_{abce}$ mutant, in which the B850 band of the LH2 complex is blue-shifted and almost degenerate with the B800 band, the LH1→LH2 excitation energy transfer was not observed nor predicted by calculations.

Introduction.

Light conditions constantly change in the natural environment and photosynthetic organisms have evolved a number of different phenotypic responses enabling them to adapt to changes in the intensity and quality of the incident light. Particularly, purple photosynthetic bacteria are able to regulate the amount of photosynthetic membranes called intra-cytoplasmic membranes (ICMs) present within their cells in response to changes in the incident light intensity (Varga and Staehelin 1983). These membranes have, depending on the species, different morphologies, such as vesicular, tubular or lamellar (Remsen 1978). In general, the lower the light intensity, the more ICMs are present. Most, but not all, purple photosynthetic bacteria have ICMs in which the photosynthetic units (PSUs) contain light-harvesting 1-reaction center 'core' complexes (LH1-RC, also called the 'core' complex) and light-harvesting 2 complexes (LH2) (Cogdell, et al. 2006; Cogdell, et al. 2004; Law, et al. 2005; Robert, et al. 2003). The number of PSUs per cell and the ratio of LH2 to 'core' complexes also vary depending on the light intensity at which the cells are grown (Aagaard and Sistrom 1972). Atomic force microscopy (AFM) studies, especially by the groups of Hunter and Scheuring, have shown that there is no area within the ICM that contains only lipid (Bahatyrova, et al. 2004; Scheuring and Sturgis 2005; Sturgis, et al. 2009) and the ratio of LH2 to LH1-RC complexes increases as the light-intensity decreases.

Bacterial light-harvesting complexes like LH2 and LH1 are membrane-bound, pigment-protein complexes in which the pigments, bacteriochlorophyll *a* (BChl *a*) and carotenoid molecules (which can be a single species or various types within a complex) are non-covalently bound at the 'correct' spacing and in the 'correct' orientation maintained by the protein scaffold. The pigments are responsible for the capture of photons and the subsequent transfer of the electronic excitation energy to the RC where it is converted into chemical energy. LH2 complexes

typically contain two populations of BChl *a*; one with its Q_y absorption band at 800 nm (B800) and the other with its Q_y absorption band at 850 nm (B850). The LH1 complex has one population of BChl *a,* which typically absorbs at ~875 nm such as in the most known bacterium *Rba. sphaeroides.* However, depending on bacterial species and chemical treatments or buffer, other spectral variants with the Q_y transition at 890, 909, 915 or even 963 nm are known (Ma, et al. 2008; Madigan 1984; Permentier, et al. 2001; Permentier, et al. 2000; Suzuki, et al. 2007). Therefore, energy transfer within the PSU flows down an energy gradient from LH2 (B800 to B850) to LH1 (B875) and finally to the RC. Interestingly the final energy transfer step is often unfavorable.

In some species of purple photosynthetic bacteria, in response to growth at different light intensities, more subtle changes take place within the PSU by modification of the spectroscopic form of the LH2 complex. For example, both *Rhodopseudomonas acidophila* (Gardiner, et al. 1993) and *Allochromatium vinosum* (Carey, et al. 2014), when grown under low-light (LL) conditions produce a LH2 complex that is characterized as B800-820 rather than B800-850, whereas *Rhodopseudomonas (Rps.) palustris* produces a B800-850 complex with a much reduced B850 absorption band (Evans, et al. 1990; Hayashi, et al. 1982b; Kiley and Kaplan 1987).

An LH2 complex is a ring structure of repeating heterodimeric units composed of one α- and one β-polypeptide, along with three BChl *a* and one carotenoid (Koepke, et al. 1996; McDermott, et al. 1995). The α- and β-polypeptides that comprise these heterodimer building blocks are approximately 7-5 kDa in molecular weight and are encoded by the *puc*BA genes (Kiley and Kaplan 1987; Leblanc and Beatty 1993; Youvan and Ismail 1985). The different spectroscopic forms of LH2 result from the expression of different *puc*BA genes and incorporation of their respective polypeptides into new LH2 complexes with altered near infra-red absorption bands

(Gabrielsen, et al. 2009). The complication induced by the presence of multiple types of α- and β-polypeptides within a single LH2 complex ring makes it difficult, in the absence of high-resolution structures, to understand the exact contribution of each *puc*BA gene pair to the overall spectroscopic form of LH2. The absorption spectrum of the complex depends not only on the amino acid compositions of the different apoproteins present (Fowler, et al. 1995) but also how the polypeptides are arranged, relative to each other (Brotosudarmo, et al. 2009). *Rps. palustris* has a multigene family of five *puc*BA gene pairs encoding the LH2 apoproteins called *puc*BA_a to *puc*BA_e respectively (Tadros and Waterkamp 1989), with *puc*BA_c presumed to be a pseudogene that is unable to form a functional LH2 complex. The LH2 from *Rps. palustris* is heterogeneous with α- and β-apoproteins encoded by different *puc*BA genes (Tadros, et al. 1993). The spectroscopic form of this heterogeneous LH2 depends upon the exact disposition of the different types of apoprotein around the ring. The current working hypothesis, derived from mass spectrometry analyses (Brotosudarmo, et al. 2011) is that the high light (HL) form of LH2 contains mainly the polypeptides from *puc*BA_a and *puc*BA_b with minor amounts, if any, polypeptides from *puc*BA_d and that the LL form of LH2 contains mostly polypeptides from *puc*BA_d with minor amounts from *puc*BA_a and *puc*BA_b (Brotosudarmo et al. 2009). To understand the role each gene pair plays in determining the LH2 phenotype in *Rps. palustris* under different light conditions, a genetic dissection strategy has been adopted to create bacterial mutants via *puc*BA deletion in all possible combinations. The quadruple *Rps. palustris* mutant with *puc*BA_a, *puc*BA_b, *puc*BA_c and *puc*BA_e gene pairs deleted (Δ*puc*BA_{abce}) reveals only the *puc*BA_d gene pair remaining in the genome and produces a LH2 complex with unprecedented phenotypic and spectroscopic properties (Southall, et al. 2017). The absorption spectrum of this LH2 complex, subsequently referred to as PucD LH2, is only produced under LL growth conditions and has a single, well-defined band at

803 nm. A high resolution structure for PucD LH2 is not yet available but the 4.71 Å structure (Southall, et al. 2017) has shown the complex to be a nonamer, very similar to the well-known LH2 structure from *Rps. acidophila* 10050 (McDermott, et al. 1995). In the PucD LH2 the excitonic coupling of the 'B850' ring BChl *a* is weak and "B850" absorption band is barely red-shifted and the B800 and "B850" bands are practically energetically degenerate resulting in a single absorption peak.

Previous studies demonstrated that alteration in the absorption spectrum of the LH2 complex has implications in energy migration and funneling in the PSU. In LL grown cells, energy transfer between the LH2 complex and LH1 is slightly reduced in the LH2→LH1 direction and is very strongly reduced in the LH1→LH2 direction. In HL adapted ICMs there is the possibility that the RC will be already 'closed' when the energy from an absorbed photon reaches LH1. If this occurs, LH1→LH2 energy transfer can take place and excitation can be transferred to another LH1-RC with an 'open' RC (Deinum, et al. 1991; Lüer, et al. 2015; Moulisova, et al. 2009). However, in low light (LL) RCs are generally 'open' and the scarce photons should be used as efficiently as possible. The spectral properties of the LH2 complex are modified and once the absorbed energy reaches LH1, the energy transfer to LH2 is energetically unfavorable (slower) and the excited state 'waits' on LH1 until it can be used by the RC.

Due to the unusual spectroscopic features of the PucD LH2 complex, the ICM from the quadruple Δ*puc*BA$_{abce}$ mutant provides another interesting system to study the energetic interaction between different LH2 spectroscopic phenotypes and LH1 complexes in the photosynthetic membrane. Even more, alteration of LH2 absorption and its effect on LH1-LH2 inter-protein excitation energy transfer can now be studied in broader aspects, as ICM samples from the same purple bacterium with multiple LH2 spectroscopic variants are now available. In

this work, spectroscopic investigations on three different types of *Rps. palustris* ICMs from (i) wild type (WT) cells grown in HL, developing the typical B800-850 LH2 complex, (ii) WT cells grown in LL, developing the LH2 complex with a reduced strength of the B850 band and (iii) Δ*puc*BA$_{abce}$ mutant producing PucD LH2 complexes. Excitation energy transfer between both LH1 and LH2 complexes has been studied using femtosecond time-resolved absorption at room temperature (RT) and for WT HL and LL ICMs at 77 K.

Materials and Methods.

Bacterial culture conditions and membrane preparation

Cells of WT and Δ*puc*BA$_{abce}$ *Rps. palustris* were cultured in C-succinate media (Gest and Bose 1963) in flat glass bottles at 30 ºC under anaerobic conditions with illumination provided by incandescent bulbs. HL conditions corresponds to 50 µmol photons $s^{-1}m^{-2}$ and LL conditions to 3 µmol photons $s^{-1}m^{-2}$. Fully adapted cells were harvested by centrifugation, washed in 20 mM MES, 100 mM KCl, pH 6.8 and then either used immediately or stored at -20 °C until required (Evans, et al. 1990). The cells, re-suspended in 20 mM Tris-HCl pH 8.0, homogenized with the addition of ~100 µg of DNase and a few mgs of $MgCl_2$, were disrupted by two passages through a French pressure cell (~15,000 psi). The ICMs were then immediately pelleted by ultracentrifugation (180,000 × g, 90 min, 4 ºC). The supernatant was discarded and the membranes gently re-suspended in 20 mM Tris-HCl pH 8.0 buffer and adjusted to an optical density at 850 nm of 50 cm^{-1}. The LH1-RC and spectral variants of LH2 complexes were purified as described previously (Roszak, et al. 2003; Southall, et al. 2017).

Spectroscopic methods

Steady-state, room-temperature (RT) and 77 K absorption spectra were recorded using a UV-1800 spectrophotometer from Shimadzu. Fluorescence emission spectra were recorded using an RF-6000 spectrofluorometer from Shimadzu. The cryogenic measurements were carried out using a VNF-100 liquid nitrogen cryostat from Janis (Janis, USA). The samples were placed in 1 cm PMMA cuvettes in 60/40 glycerol/buffer (v/v) mixture and slowly frozen.

Transient absorption (TA) experiments were carried out using Helios, a femtosecond time-resolved and pump-probe absorption spectrometer (UltrafastSystems, LCC) coupled to a Spectra-Physics femtosecond laser system described in detail previously (Niedzwiedzki, et al. 2016). In order to minimize excited state annihilation on BChl *a* rings in either LH2 or LH1, the energy of the excitation beam (800 nm) was set low to 20-40 nJ corresponding to $3\text{-}7\times10^{13}$ photons/cm^2 per pulse. For RT studies, the sample was placed in a 2 mm quartz cuvette and vigorously stirred with a magnetic stirrer in order to avoid permanent photodamage to the sample.

Data processing and analysis

Temporal dispersion in the TA datasets was corrected using Surface Xplorer software (UltrafastSystems LCC). Transient absorption signal at any time delay and wavelength, $\Delta A(t,\lambda)$ can be decomposed to superposition of n^{th} $C_i^S(t)\cdot SADS_i(\lambda)$ (Species Associated Difference Spectra) products (van Stokkum, et al. 2004)

$$\Delta A(t,\lambda) = \sum_{i=1}^{n} C_i^S(t) SADS_i(\lambda)$$

where $C_i^S(t)$ are time-dependent SADS concentration defined by kinetic model mimicking true excitation decay pathway. TA datasets were initially fitted with a simple kinetic model assuming sequential decay of excitation in subsequently slower steps, giving so-called EADS (evolution associated difference spectra) (van Stokkum, et al. 2004) and then simulated using anticipating kinetic model hypothetically mimicking true multi-direction decay pathway of excitation. Those

kinetic analyses were done using CarpetView software (Light Conversion Ltd.). The concentration of the initially populated EADS/SADS was convoluted by the instrument response function (IRF) simulated by Gaussian with the full width at half maximum (FWHM) of ~200 fs. Calculations of Förster energy transfer rate for the LH1→LH2 route were performed using PhotochemCAD 2 software (Dixon, et al. 2005).

Results

Steady-state absorption

Figure 1 illustrates changes in absorption spectra of the *Rps. palustris* ICM from WT and Δ*puc*BA$_{abce}$ mutant when cells are grown in high and low light-intensities. In HL, the absorption spectrum of the ICM is dominated by the 'standard' LH2 B800-850 type complex with absorption bands at approximately 803 and 863 nm. The shoulder on the red edge of the B850 band is associated with the LH1-RC complex with an absorption maximum at ~880 nm. In LL, the relative height of the peak at ~860 nm is substantially reduced and the band at 803 nm concomitantly increased. These changes reflect the incorporation of the LL-version of the LH2 complex into the membrane. In HL, the LH2 complex contains primarily the *puc*BA$_a$ and *puc*BA$_b$ polypeptides but as the light intensity decreases, these are progressively replaced by *puc*BA$_d$ polypeptides resulting in the distinctive spectrum for this complex. The absorption spectrum of the Δ*puc*BA$_{abce}$ mutant grown at HL does not reveal absorption bands from the LH2 complex as there is no expression of the *puc*BA$_d$ gene pair, and therefore contains only the LH1-RC 'core' complex. This spectrum was omitted as it essentially mimics the LH1-RC absorption spectrum. At LL conditions, in the ICM of Δ*puc*BA$_{abce}$ mutant the PucD LH2 is produced and the absorption spectrum (Figure 1C) exhibits maxima at 808 and at 881 nm at RT and at 804 and 897 nm at 77 K. These bands originate from PucD LH2 and the LH1-RC complexes, respectively.

An interesting aspect is how well the absorption spectra of LH2 and LH1-RC complexes obtained via detergent treatment of the ICM membranes correspond to their membrane-embedded counterparts. Typically, it is assumed that detergents (*n*-Dodecyl-β-D-maltoside (DDM) and/or N,N-Dimethyldodecylamine N-oxide (LDAO), which are commonly used for purification of LH2 or LH1-RC), do not significantly alter their absorption spectra, which are only energetically offset due to the different refractive index of the medium. Here it could be tested across multiple spectral forms of LH2 complexes at both RT and 77 K. This analysis is shown in Figure 2, which provides absorption spectra of the ICMs and traces reconstructed from their principal components – absorption spectra of individual LH2 and LH1-RC resuspended in buffer. Since the spectra of the separated proteins are blue-shifted in respect to the membrane-embedded complexes, it was necessary to shift them energetically toward lower energies on the scale converted to wavenumbers (to avoid nonlinearity of the wavelength scale). The ICM absorption spectra are mimicked as the weighted sum of the LH2 and LH1-RC absorption spectra. The best agreement with the ICM spectrum was achieved for the LL ICM from the WT strain. This finding is in agreement with similar attempts done previously on the LL *Rps. palustris* ICMs at RT (Hayashi, et al. 1982a). At 77 K, in the absorption of the HL ICM, the B800 band deviates in position from what is expected based on spectral reconstruction (~7 nm difference). It suggests that the detergent/buffer environment does not electrostatically complement the membrane in this case. Although this effect is not clearly recognizable at RT, it apparently appears at cryogenic temperatures. The most interesting point is the outcome of the 77 K reconstruction of the LL ICM from Δ*puc*BA$_{abce}$ mutant. It suggests that the membrane spectrum comprises an additional absorption band at ~813 nm (extra green peak in Figure 2F) that cannot be associated with any spectral feature from either PucD LH2 or LH1-RC. This effect is clearly observed at cryogenic temperatures but is difficult to observe at

RT. It is possible that either in the membrane PucD LH2 exists in two spectral versions or the B850 and B800 bands are not as completely degenerate in the membrane as they are in the buffer.

Previous investigations demonstrated that the LH2/LH1-RC ratio changes with light conditions and is higher in LL (Aagaard and Sistrom 1972). The spectral reconstructions of absorption spectra from various ICMs provided in Figure 2 allow more insight on this subject to be obtained. Since the contribution of the absorption spectrum of the core complex is well-defined and identical in all those membranes, the ICM absorption spectra could be corrected for the scattering effect ($\sim\lambda^{-4}$), overlaid and accordingly adjusted to the same level of LH1-RC contribution. This is shown in Figure 3. It indeed shows that the LH2/LH1-RC ratio is higher in the LL adapted ICMs. Since the spectral properties of the BChl *a* Soret band should not be affected at LL, change in its amplitude could be used to find a relative change in the ratio of the two complexes. By subtracting the contribution of LH1-RC from each spectrum and then dividing the LL spectra by the HL spectrum (all are LH1-RC-free) a relative change in LH2/LH1-RC ratio can be calculated. It shows that the WT LL ICM contains ~1.5 times more LH2 complexes than the HL counterpart. It would be useful to convert this relative ratio into an actual LH2/LH1-RC ratio. The AFM studies of the intact patches from LL ICMs of *Rps. palustris* show that complex packing in the membrane may not be homogenous and some areas show clustered multiple LH2 complexes while others have both LH2 and LH1-RC complexes randomly distributed, in an average ratio of 3:1. Interestingly the AFM images of patches of the HL ICMs also show large areas of closely packed monomeric LH1-RC complexes and no LH2 (Scheuring, et al. 2006). However, it is worth noting that selected AFM images do not always represent the bulk distribution of antenna complexes in the ICM of living cells and that such images should certainly not be interpreted as unambiguously correct in all cases. Therefore, if on average a random distribution of complexes

is more representative, and because LL ICM always has more LH2 complexes, an LH2/LH1-RC ratio of 2:1 or less should be characteristic for the HL ICM. Comparable values were obtained from reconstruction of the BChl *a* Soret band of the ICM absorption spectrum. This band is least affected by excitonic interactions between BChls and its absorbance value can be straightforwardly used for calculation of the BChl *a* content in each LH1-RC and LH2 complex. Assuming, for example, that absorption spectra from Figure 3 corresponds to membrane area consisting of only one LH1-RC (ie. normalization to one LH1-RC), the absorbance level of the Soret band in the LH1-RC absorption spectrum will correspond to 34 BChls (30 from LH1 15-mer and 4 from RC). Then the remaining absorbance can be converted to numbers of BChls residing in the surrounding LH2s. Taking into consideration that in HL and in LL ICMs the LH2 is in form of a nonamer (total of 27 BChl *a*), previous AFM investigations suggested that LL LH2 is an octamer (Scheuring, et al. 2006) but recent crystallographic data does not support this (Southall, et al. 2017), the LH2/LH1-RC ratios will be as follow: 2:1 for the HL ICM and 2.8:1 for the LL ICM. This is in perfect agreement with previous estimates.

Transient absorption

Transient absorption spectra of the HL ICM taken at RT and at 77 K upon excitation at 800 nm are given in Figure 4. Immediately after excitation, (120 fs TA spectrum) bleaching of the B800 LH2 band is observed. It is also accompanied by another weaker, broader bleaching that is centered at ~870 nm and likely corresponds to initial collective bleaching of B850 and B875 from a direct excitation of the higher excitonic band of the B850 exciton and the blue edge of the B875 absorption band of the LH1-RC. As time progresses, bleaching of the B800 band diminishes quickly (420 fs and 2 ps TA spectra) and bleachings of the B850 and B875 bands rise. Those dynamic features indicate an ultrafast energy transfer from excited B800 BChl *a* (B800*) to B850

and beginning of the subsequent B850*→B875 energy transfer step. In RT data, within 50 ps the recovery of bleaching of the B850 band is almost complete. This process takes longer at 77 K. Based on spectral judgement, it is not clear if the cryogenic temperature affects the dynamics of those two steps in this membrane. It should also be noted that while bleaching of the B800 band quite adequately mimics the mirrored steady-state absorption of the B800 band, minima in the B850 and B875 bleachings are red-shifted compared to the maxima of steady-state absorption of those bands (see also Figure 2). This is because as well as the real absorption bleachings, a probe-driven stimulated emission (red-shifted) with similar amplitude is present. In addition, both B850* and B875* have excited state absorption bands positioned at the short wavelength edge of the steady-state absorption band. This positive signal asymmetrically compensates for the bleaching of B875 and together with the stimulated emission causes the observed bleaching band to be significantly red-shifted with respect to the steady-state absorption band. There is no evidence that under the applied experimental conditions (1 kHz laser, small sample volume, same excitation spot at 77 K, plain buffer), that any remaining bleaching of the RC after the decay of B875* is present. This indicates that instantaneously, the whole population of RCs converts to the "closed" state and essentially becomes silent in TA measurements due to their permanent bleaching (800 nm excitation will directly and efficiently excite the RC, see Figure 3A). Under this scenario, excitation cannot be further transferred to the RC and remains on B875 BChl *a* and has to either decay intrinsically to the ground state or, if possible, transfer to an LH2 complex. Occurrence of this latter event (an additional kinetic component in TA dynamics) should be clearly distinguishable between samples. Since the energetic gap between the "B850" and B875 bands increases in the LL ICM, simultaneously the probability of the transfer should decrease.

Alteration of the LH2 complex to the one with a diminished B850 band, such as that present in the LL ICM from WT *Rps. palustris*, has clear impacts on the rate of B850*→B875 energy transfer as observed in TA results in Figure S1. It is difficult to spot in the congested TA spectra but it is very apparent in the kinetic trace highlighting the initial rise of bleaching of the B875 band at 909 nm. The rise of bleaching is associated with the process of excitation transfer from the spectrally altered LH2 complex. The process is elongated and the bleaching reaches a minimum after ~20 ps in comparison to ~6 ps for the HL counterpart. Even though steady-state absorption shows that B850 and B875 overlap, the TA spectra of the LL WT *Rps. palustris* membrane show substantially better spectral separability at 77 K compared to the HL counterpart. Bleaching minima (observed not nominal) of B850 and B875 bands could be clearly resolved at 871 nm and 907 nm, at positions that are red-shifted with respect to their maxima in the absorption spectrum due to the abovementioned reasons.

Transient absorption results of the most interesting ICM from the Δ*puc*BA$_{abce}$ *Rps. palustris* strain in which both B800 and B850 bands seem to be degenerate are given in Figure S2. Due to ideal spectral overlap of the hypothetical fluorescence spectrum of the B800 band and "B850" absorption, the B800*→"B850" energy transfer is nearly instantaneous and the initial bleaching of the B800 band could not be resolved by the spectrometer. At RT, within 200 fs, bleaching of overall B800-"B850" band evolves to the narrow band with a minimum at ~821 nm, suggesting that after compensating for the red shift caused by stimulated emission, the steady-state absorption of the "B850" band could be centered at ~815 nm. Widening of the energetic gap between "B850" and B875 has a pronounced effect on the "B850*"→B875 energy transfer rate. The rise time of the B875 bleaching is further elongated; at RT the bleaching reaches a minimum at 40 ps after excitation.

In order to visualize changes in the rise time of the B875 band in the studied ICMs, the RT 909 nm traces were fitted and the results are shown in Figure S3. Positive components are associated with a rise of bleaching of the signal at 909 nm, and negative components are associated with decay of the signal (recovery of bleaching). Two rise components are present in TA traces from WT HL and LL samples. One has essentially the same lifetime of ~1.2 ps and is very likely associated with the rise of bleaching of the B850 band (due to energy transfer from B800) that could be still detectable at this wavelength in these membranes. This signal is not present in the ICM from the Δ*puc*BA$_{abce}$ mutant as the "B850" band is blue-shifted and does not overlap with the B875 band (see Figure 2). Note that the contribution of this component is the largest for the HL sample but if the B850 band diminishes (LL sample) it becomes smaller. The second rise component is associated with LH2→LH1 excitation energy transfer and its lifetime (8 ps, 9.9 ps, 12 ps for HL, LL WT and LL mutant samples, respectively) apparently depends on the energetic gap between the "B850" and B875 bands. Since this time constant is the same for the B850 band bleaching recovery (decay) as for the B875 bleaching rise, both contributions may compensate in spectral ranges in which B850 and B875 absorption bands overlap and the "effective" rise component will be small (see blue trace for WT HL). This was also the reason for probing those transient signals at the long wavelength edge of the B875 band in which the rise of the B875 bleaching should dominate. The WT samples show two decay components, but only one is detectable for the LL mutant. The longer-lived component has a very similar lifetime of 200-250 ps in all samples and corresponds to the intrinsic decay of the LH1 complex with closed RC as demonstrated previously (Ma, et al. 2008). The second decay component is present only in WT LL and HL samples but its lifetime is significantly shorter for HL ICM (45 ps vs 80 ps). In addition, its contribution in the overall transient signal is also larger in the HL sample. It strongly suggests

that this accelerated recovery of the LH1 bleaching is associated with LH1→LH2 excitation energy transfer, as no other de-excitation pathways are expected in those samples under the applied experimental conditions. In order to gain more insight into the dynamics of the system, the TA single wavelength fitting procedure can be extended toward the whole spectral range with the application of global analysis.

Global analysis of TA results

In order to gain more information about dynamic characteristics of TA data of the ICMs, the whole datasets were analyzed globally. The datasets were fitted with a model assuming sequential decay of excitation with decreasing, irreversible rates (increasing lifetimes), which is more intuitive than the physically unrealistic sum of exponential decays as used for single wavelengths fits in Figure S3. Note that this model will still only partially mimic the expected migration pathway of an excitation that in an idealized scenario has a sequential pattern of B800*→B850*→B875*→B875 (ground state), therefore the spectral amplitudes obtained from the fitting should not be assigned to individual molecular species (B800, B850, etc.). However, as the single wavelength fits suggest, the last step is more complicated for the WT ICMs due to more possibilities that arise if an additional B875→B850 route is accessible. Global fitting results of TA data with this model are commonly abbreviated as EADS (evolution associated difference/decay spectra) (van Stokkum, et al. 2004). The EADS profiles obtained from global analysis of RT TA of the ICMs from this work are shown in Figure 4, 77 K EADS are given in Figure S4. Note that in this fitting model, the lifetime decay of the former EADS is the rise time of the later one. The first EADS clearly is associated with decay of the B800 band initially populated by excitation. The lifetime of 1.1-1.4 ps of B800* BChls is in agreement with the value known from multiple previous studies (Herek, et al. 2000; Ma, et al. 1997; Scholes and Fleming 2000; Wu, et al. 1996). The

EADS with lifetime of 8.6-15.7 ps corresponds to the decay of the B850 band. Global fitting results confirm that the lifetime of B850* BChl *a* lengthens if the B850 band is diminished or blue-shifted (WT LL, and Δ*puc*BA$_{abce}$ LL). The final two EADS (only one for Δ*puc*BA$_{abce}$ LL) share very similar lineshapes, indicating that both components are associated with the same excited state, namely B875*, decaying with different rate constants. This is where the model most likely fails to mimic the actual excitation decay pathway, the faster EADS components (48 ps and 86 ps) probably correspond to energy transfer from LH1 to LH2 and the whole kinetic model should be rebuilt. Note that temporal characteristics of the data may also contain information about subsequent energy transfer to another LH1' complex that could occur after repopulating LH2 but this is not evident in the simplistic sequential imitation of the excitation transfer/decay. This issue will be addressed further in the discussion, in which more sophisticated kinetic models are provided to more realistically simulate the TA data.

Discussion

LH1→LH2 excitation energy transfer

The most widely accepted reason for the drastic changes in steady-state absorption of LH2 complexes upon change of the light conditions at which cells are grown is the adjustment of LH2→LH1 and LH1→LH2 excitation energy transfers. Under HL conditions, RC turnovers from a "closed" to an "open" state are not able to keep up with the avalanche of excitations trying to enter the RC from the surrounding LH1 complex. If it happens, the best way to utilize those extra excitons is to temporarily redirect them to another complex (LH1') in the hope that those could be used by another RC that will be in the "open" state. Ideally, LH1→LH1' hopping will be the most efficient way to transfer excitations, however due to ICM organization an LH1→LH2→LH1'

sequence is also very probable and in many cases the most probable, due to spatial separation of neighboring LH1-RC complexes.

However, a basic question that could be asked here is if LH1→LH2 energy transfer is energetically possible and if so is it an LH1* deactivation route that should be considered or could it be neglected. If only nominal excitonic energies of LH1 and LH2 (absorption maxima) are taken under consideration, energy transfer from LH1* to LH2 would require the B875* exciton being isoenergetic with LH2 B850. The fraction of LH1* that will have adequate thermal energy at either RT (293 K) or at 77 K could be calculated based on the ratio, R, of Boltzmann distribution for those two energetic states (EB875, EB850):

$$R = e^{\frac{E_{B875} - E_{B850}}{k_B T}} \quad (1)$$

Where T is temperature and k_B is Boltzmann constant. E_{B875}-E_{B850} = -0.039 eV (-0.036 eV) at 293 K (77 K) and R_{RT} = 21% and R_{77K} = 0.45%. It shows that at RT the LH1* to LH2 route will have a substantial contribution in LH1* deactivation, however the fraction of LH1* with LH2-like energy would be essentially negligible at 77 K, thus LH1-to-LH2 energy transfer should not play any role in de-excitation of the LH1* at cryogenic temperatures.

However if experimental data, LH2 absorption and LH1 emission are taken under consideration, reflecting complex-to-complex heterogeneity in excited-state energies, energy transfer rates could be calculated employing resonance energy transfer mechanism. The inter-protein BChls, or more precisely B875 and B850 excitons (dimers of strongly coupled inner-protein BChls) are weakly coupled and Förster resonance energy transfer could be used to approximate excitation energy transfer between complexes (between B875 and B850 dimers). Consequently, the spectral overlap between the LH1 B875 band's fluorescence and LH2 B850 band's absorption and inter-complex distance would play crucial roles in the efficiency of this

process. Simple calculations can show that efficiency of this route of the excitation pathway could be quite considerable.

For weakly coupled systems, the energy transfer rate is described by the equation for the Förster resonance transfer rate:

$$k_{ET} = 8.8 \times 10^{23} \frac{\kappa^2 \phi_{f(D)}}{n^4 \tau_D R^6} \int_0^\infty \frac{F_D(v)\varepsilon_A(v)}{v^4} dv \quad (2)$$

where κ^2 is relative orientation of the donor and acceptor transition dipole moments (B850 and B875), $\Phi_{f(D)}$ is the donor (B875) fluorescence quantum yield, τ_D is the donor (B875) fluorescence lifetime in the absence of acceptor (B850), n is the refractive index of the environment, R is the donor-to-acceptor (B875-to-B850) center-to-center distance and the integral determines the spectral overlap between the normalized fluorescence spectrum of the donor (B875, $\int_0^\infty F_D(v)\, dv = 1$) and the molar absorption coefficient ε(ν) of the acceptor (B850). Previously, ε(λ = 850 nm) was determined for B850 of the LH2 from *Rb. sphaeroides* (ε(850) = 184,000 $M^{-1}cm^{-1}$) (Clayton and Clayton 1981) and due to spectral and structural similarities with the HL LH2 studied here this value can be used as a reference ε at the maximum of the B850 band. The whole $\varepsilon_{HL}(\lambda)$ spectrum of the B850 band can be obtained from reconstruction of the absorption spectrum into individual B800 and B850 components and neglecting the B800 contribution. However, ε(λ) is not known for B850 from the LL LH2. This problem can be bypassed by normalizing both HL and LL LH2 absorption spectra at the carotenoid band at which, due to similarities in both complexes (1 identical carotenoid per 3 BChls), the spectra are expected to be the same in amplitude and shape (spectra will be normalized to 1 carotenoid-3 BChls unit). Then, $\varepsilon_{LLB850}(\lambda)$ could be simply calculated from the proportion in B850 bands of both complexes. This gives $\varepsilon_{LL}(850)$ = 66,500 $M^{-1}cm^{-1}$ (maximum of the band). Both extinction coefficients (as a function of

wavenumber) are given in Figure 6A. Note that the PucD LH2 from the LL Δ*puc*BA$_{abce}$ ICM is not provided as the spectral overlap will be negligible.

Other parameters were assumed as follows: The fluorescence spectrum of the B875 (Figure 6A red profile) was measured separately for the individual LH1-RC complex and then energetically shifted to match its expected position of 890 nm in the ICM membrane at RT (Hayashi, et al. 1982a). The spectral overlaps are given as shadowed profiles. The distance between donor and acceptor (between B875 and B850 dimers) was set to 22 Å, identical to that used in theoretical modelling of the inter-complex excitation energy transfer published previously. This distance gave minimized van der Walls interactions between complexes (Ritz, et al. 2001). To make it more intuitive, an illustration of a hypothetical spatial arrangement of LH2 and LH1 complexes is also provided (Figure 6B). It is based on the 1KZU LH2 crystal structure from *Rps. acidophila* 10050 (Prince, et al. 1997) and the 1PYH LH1-RC crystal structure from *Rps. palustris* (Roszak, et al. 2003). To get more insight about the sensitivity of the transfer rate to the inter-complex separation (which could certainly occur in a fluid membrane), calculations were also performed for a modestly longer distance of 25 Å. The refractive index was set to 1.5, an approximate value for mixed protein/membrane environment of interacting BChls (Paillotin, et al. 1998), the fluorescence lifetime of the B875 was set to 250 ps as demonstrated in dynamics of transient absorption (B875 bleaching recovery and fluorescence lifetime are equal in value) in this study and in agreement with previous findings for LH1-RC complexes with closed RCs (Ma, et al. 2008), Φ_f of B875 was set to 0.015. A literature value of ~0.02 was found (Sauer and Austin 1978), however it was obtained based on the assumption that Φ_f of pure BChl *a* in diethyl ether is 0.25 which later was demonstrated to be lower, in the range of 0.17-0.20 (Connolly, et al. 1982; Losev, et al. 1986) and the value of 0.015 used here reflects this correction. The orientation factor κ^2 was

assumed to be 2/3, the value that is typically used for randomly oriented donor-acceptor pairs. It is not quite a correct assumption as interacting BChls excitons will be in more or less fixed orientations, however, factors like membrane fluidity, and internal protein and pigment motions present at RT could efficiently perturb the rigidity and the mutual orientations of pigments in the system. Assuming a completely rigid B875-B850 assembly, more-less parallel but not collinear geometry of transition dipole moments is expected and this would give a κ^2 value close to 1. Finally, after applying calculations, the excitation transfer rates are as follows: $(5.6\ ps)^{-1}$ and $(12\ ps)^{-1}$ for HL and LL B875-B850 pair, respectively, at 22 Å separation and if that is stretched out by 3 Å values will change to $(18.5\ ps)^{-1}$ and $(40\ ps)^{-1}$ for HL and LL, respectively. These findings can be compared with some previous estimates. The theoretically derived rate of LH1→LH2 excitation energy transfer for open geometry LH1 (same as the geometry of LH1 from *Rps. palustris*) and HL-like LH2 is $(20.3\ ps)^{-1}$ (Ritz, et al. 2001). More recently, LH1→LH2 transfer rates were also experimentally studied in HL and LL ICM from *Rps. palustris*, the same as in this work. Based on kinetic modeling of the time-dependent first derivative of transient absorption spectra at certain wavelengths, it was deduced that for HL LH2-containg ICM the rate is in the $(16\text{-}20\ ps)^{-1}$ range and for the LL sample in the $(36\text{-}38\ ps)^{-1}$ range (Lüer, et al. 2012). As demonstrated above, if a small (~10%) variability of the distance between LH1-RC and LH2 complex, in respect to the most optimal, is introduced, the transfer rates estimated in this work and known from previous studies are very comparable. We have not performed any calculations for ET at 77 K because not all required experimental data are available. However, a simple approximation of the spectral overlap, as shown in Figure S6, suggests that at least for WT HL ICM, the possibility of the LH1-to-LH2 energy transfer should not be ignored.

Spectro-temporal simulation of TA results

Finally, all information on the spectral and temporal characteristics of ICM components can be used to develop a more realistic kinetic model of excitation migration within the PSU. This model should incorporate the fact that LH1→LH2 excitation energy transfer is present and is more efficient in HL ICM. The model should break macroscopic (observed) rates obtained from global and single wavelength fits into microscopic rates that will also reflect intrinsic decay rates and energy transfer routes. Such kinetic models accompanied by simulation results for RT TA of each ICM are provided in Figure 7. The simplest model of excitation migration/decay pathway was constructed for TA of the LL ICM from Δ*puc*BA$_{abce}$ mutant (Figure 7A). No spectral overlap between the LH1 fluorescence emission and the "B850" absorption band of the PucD LH2 makes everything simple for this system. The 800 nm excitation absorbed by B800 BChls is transferred to "B850" with 0.9 ps time constant. The step occurs even faster than in classical B800-850 LH2 (~1.2 ps) most likely due to the fact that both B800 and B850 bands are spectrally almost degenerate, making energy transfer faster. The observed B850* decay lifetime comprises two microscopic decays: intrinsic decay to the ground state with lifetime of 1.2 ns (Dilbeck, et al. 2016) (it could be neglected for B800* as non-competitive route) and energy transfer to B875 with time constant of 16.4 ps. The B875* upon the absence of an available RC to trap the excitation (800 nm excitation immediately bleaches RC for the time course of the experiment) is forced to internally decay back to the ground state with lifetime of ~200 ps. The LH1→LH2 transfer cannot be involved due to the lack of spectral overlap of the B875 fluorescence and blue-shifted "B850" absorption of the PucD LH2. The spectro-kinetic components from the simulation, SADS, are given in Figure 7B, the exemplary TA signal at 880 nm (the same representative wavelength for all three simulations) decomposed into contributions from individual molecular species is given in Figure 7C. For the WT LL ICM in which the B850 band is back at 850 nm but its intensity is

diminished, simulation includes population of B850* via excitation energy transfer with rate of $(93\ ps)^{-1}$ competing with intrinsic decay (250 ps) of B875* to the ground state (Figure 7D). One would question what happens after this step. It could be argued that excitation will jump back and forth within the same LH1-LH2 pair, however, on the other hand, hopping of the exciton within the B875 BChl *a* ring would be much faster and excitation could be passed to a different LH2 complex than it initially came from (there are 2-3 LH2 per 1 LH1-RC, statistically). To reflect this in the kinetic model it was assumed that excitation is passed to a different LH2 complex (LH2') that subsequently transfers excitation energy into another LH1-RC complex (LH1-RC', however it could be the same one as well). It can be imagined that this sequence will be repeated multiple times in the membrane in which tens or even hundreds of complexes are clustered together, however, contribution of each subsequent step in the overall process will be smaller and can be neglected at some point. Involving even a few such cascades into the simulating model will substantially complicate everything and make it unmanageable, but as demonstrated in Figure 7E and F, cutting the LH1-LH2-LH1 loop after the first round gives already satisfactory results. Note that in the model process the population of LH2' is much slower in respect to the subsequent step and B850'* spectrally cannot be resolved due to lack of accumulation of this spectral species. The final kinetic model, simulating dynamics of TA of the HT WT ICM is shown in Figure 7G. In this system, due to increased spectral overlaps of B850 and B875 (absorption and fluorescence, in both directions) energy transfer rates in all steps are bigger (shorter lifetimes) resulting in the most efficient energy transfer in every direction (B850 $\leftrightarrow$ B875). Unlike for LL ICM, in this system population of B850'* (bleaching) is resolved, however its contribution in the overall TA signal is still very small with respect to other components (see red trace in Figure 7I).

Excitation energy transfer calculations presented earlier in the discussion have shown that the ratio of LH1→LH2 transfer rates for WT HL and LL ICM should be ~3. Kinetic modelling of experimental results demonstrates that this ratio will be ~2.2. In this context, both predictions and experimental outcomes are not far away from each other and seem to be quite feasible.

Very likely "forward" LH2→LH1 and "backward" LH1→LH2 energy transfers lead to energy transfer equilibrium. It is not quite certain if the requirements for equilibrium, $k_{LH1\rightarrow LH2}[LH2] > k_{LH1}$ and $k_{LH2\rightarrow LH1}[LH1] > k_{LH2}$ (where [LH1] and [LH2] are complex's concentrations and k_{LH1}, k_{LH2} are intrinsic decay rates to the ground state) are actually met. Most likely, it is correct for LH2→LH1 transfer, however it is uncertain for the LH1→LH2 transfer rate. However, if it is assumed that equilibrium is actually formed, the free energy for energy transfer could be calculated via the equation:

$$\Delta G_{ET} = \Delta H_{ET} - T \cdot \Delta S_{ET} = -R \cdot T \cdot ln\frac{k_{LH1\rightarrow LH2}}{k_{LH2\rightarrow LH1}} - T \cdot k_B \cdot \ln\frac{N_{B850}}{N_{B875}} \quad (3)$$

Where $\frac{k_{LH1\rightarrow LH2}}{k_{LH2\rightarrow LH1}}$ is an equilibrium constant, *R* is the universal gas constant of 8.314 J/mol and ($k_B \cdot \ln\frac{N_{B850}}{N_{B875}}$) corresponds to the change in statistical entropy of both systems (LH1 and LH2) assuming that numbers of B850 and B875 dimers ($N_{B850,B875}$) correspond to the number of microscopic states of those systems. The enthalpic contribution is 4.1 kJ/mol (for $k_{LH1\rightarrow LH2}$ = (43 ps)$^{-1}$, $k_{LH2\rightarrow LH1}$= (7.6 ps)$^{-1}$ taken from the target analysis) and the entropic contribution is ~0.9 kJ/mol, thus ΔG_{ET} is ~5 kJ/mol.

Conclusions

In this study, various spectroscopic investigations on three ICMs from two strains of the photosynthetic purple bacterium *Rps. palustris* containing an identical LH1-RC complex but various spectroscopic forms of LH2 complex have been performed. The studies focused on inter-

protein excitation energy transfer and how it is affected by changes in spectroscopic features of the LH2 complex. The studies particularly focused on LH1→LH2 excitation energy transfer. That is strongly affected if the LH2 complex alters its spectroscopic signature and modifies the oscillator strength and position of the B850 band. Calculations of excitation energy transfer with application of the Förster mechanism and further kinetic simulations of transient absorption datasets demonstrated that in the HL form of the WT ICM the rate of the LH1→LH2 transfer will be 2-3 times faster compared to the LL form of the ICM from this strain. In the ICM from Δ*puc*BA$_{abce}$ mutant in which the B850 band of LH2 complex is blue-shifted and almost degenerate with B800, the LH1→LH2 transfer is not observed nor was predicted from calculations. Based on those and previous studies it could be concluded that the ability to efficiently redirect excitation in HL conditions has a big advantage to prevent photo-saturation of the RC complex as well as minimizes the waste of excitations that could accumulate on the LH1 B875 ring in multiple centers and eventually annihilate. In the LL ICMs, which are exposed to low light and photons that could be absorbed are substantially limited, every excitation counts and redirecting the excitation pathway to the LH2 complex is not necessary and energetically not practicable as it could generate additional excitation losses.

Acknowledgements

This work was supported by the Photosynthetic Antenna Research Center, an Energy Frontier Research Center funded by the U.S. Department of Energy, Office of Science, Office of Basic Energy Sciences under Award Number DE-SC 0001035.

Figures and Figures Captions

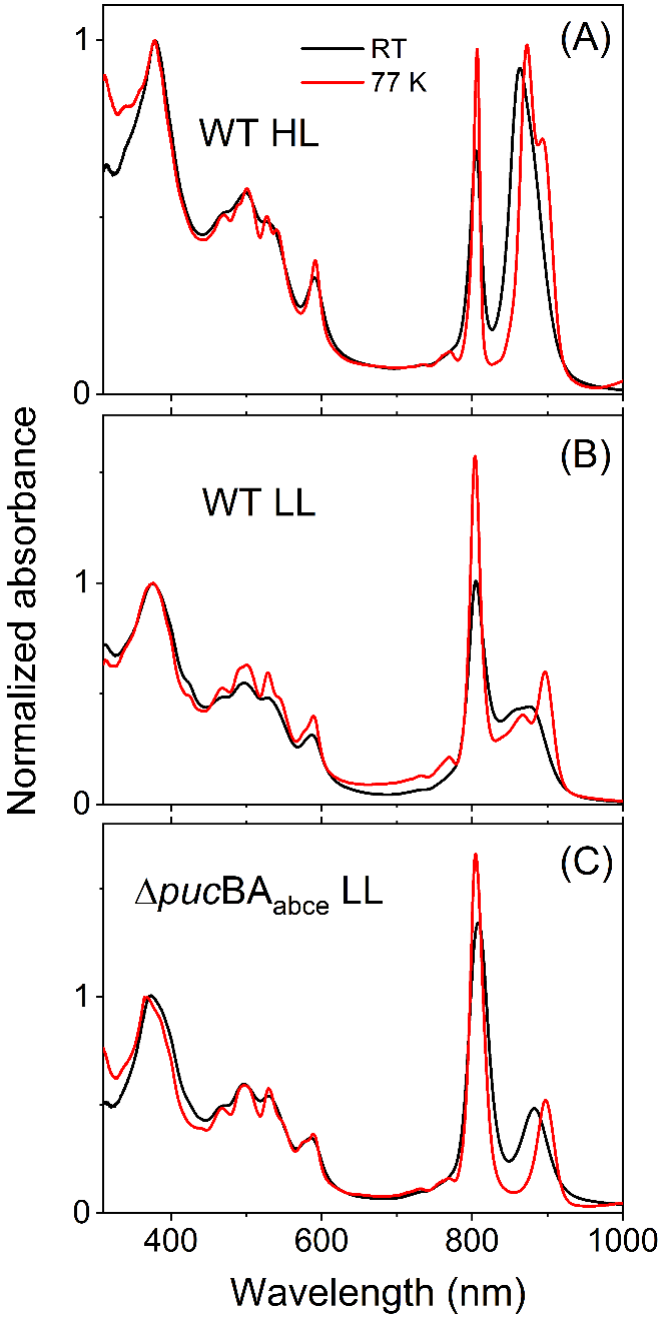

Fig. 1 Room temperature and 77 K absorption spectra of the ICMs from WT *Rps. palustris* grown under white light from (A) HL, (B) LL and (C) from Δ*puc*BA$_{abce}$ mutant grown in LL conditions. The Δ*puc*BA$_{abce}$ mutant grown in HL produces ICM with LH1-RC only and is not shown here

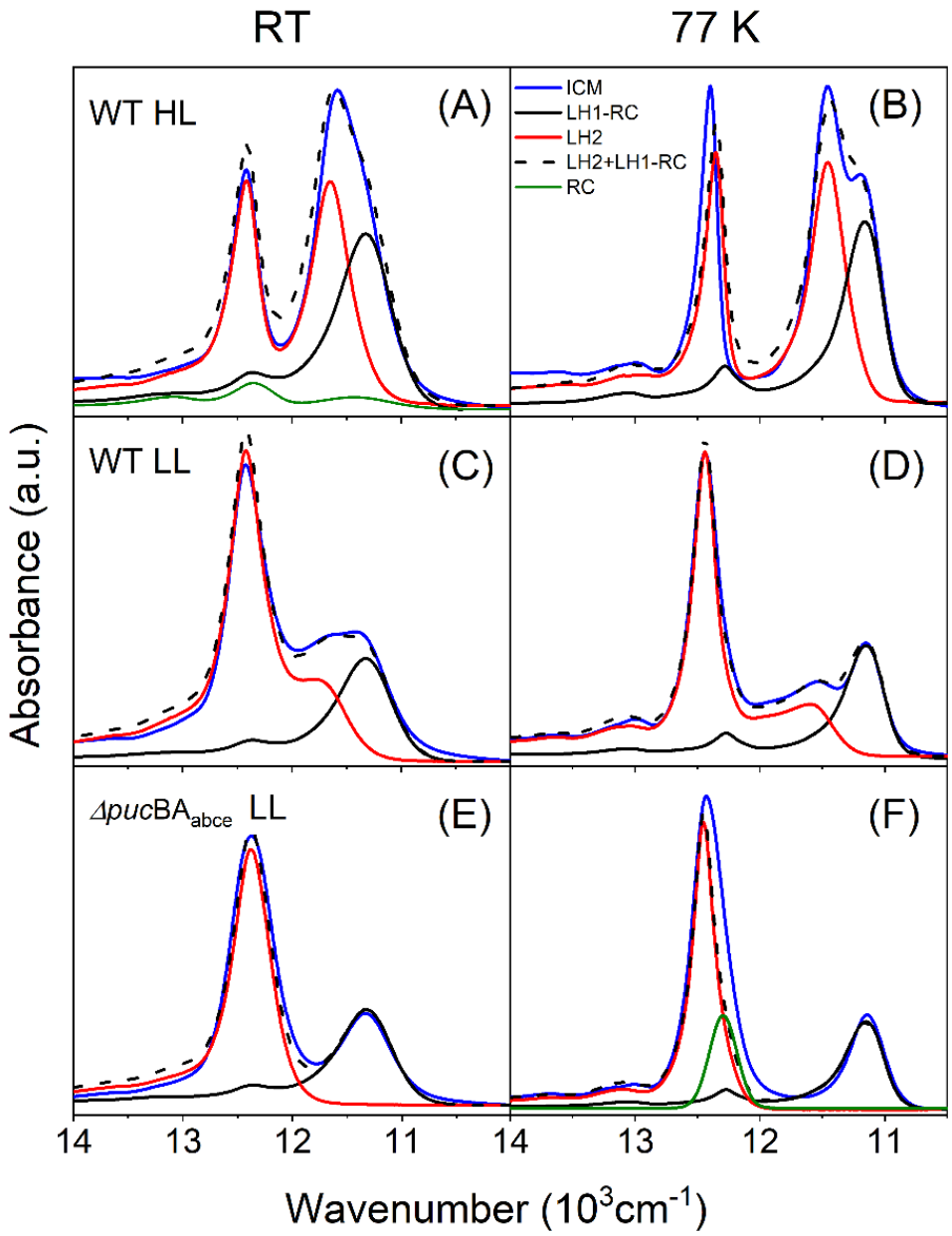

Fig. 2 Spectral reconstruction of (A, C, E) RT and (B, D, F) 77 K absorption spectra of the ICM from their principal constituents, the absorption spectra of individual LH2 and LH1-RC complexes. The reconstructed spectra are plotted in dashed black lines. The green band in panel F corresponds to a Gaussian curve that needs to be added in order to correctly reconstruct the ICM absorption spectrum.

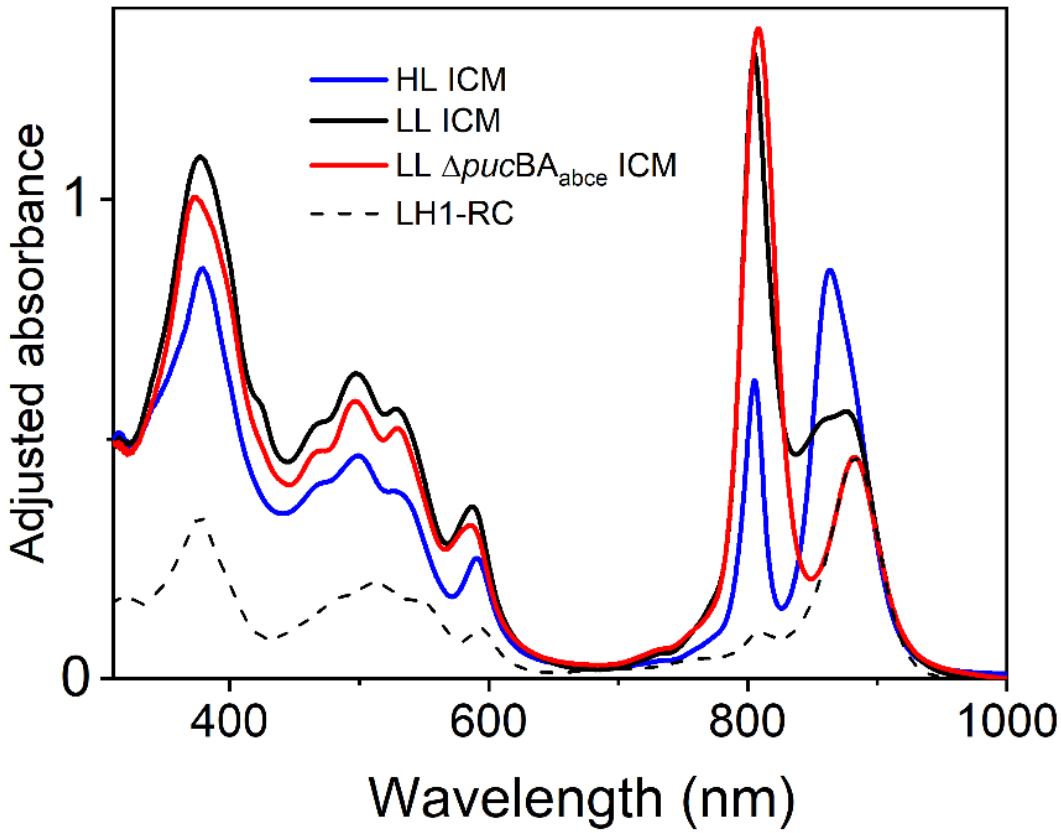

Fig. 3 The RT absorption spectra of studied ICMs corrected for scattering and adjusted to the same level of LH1-RC contribution

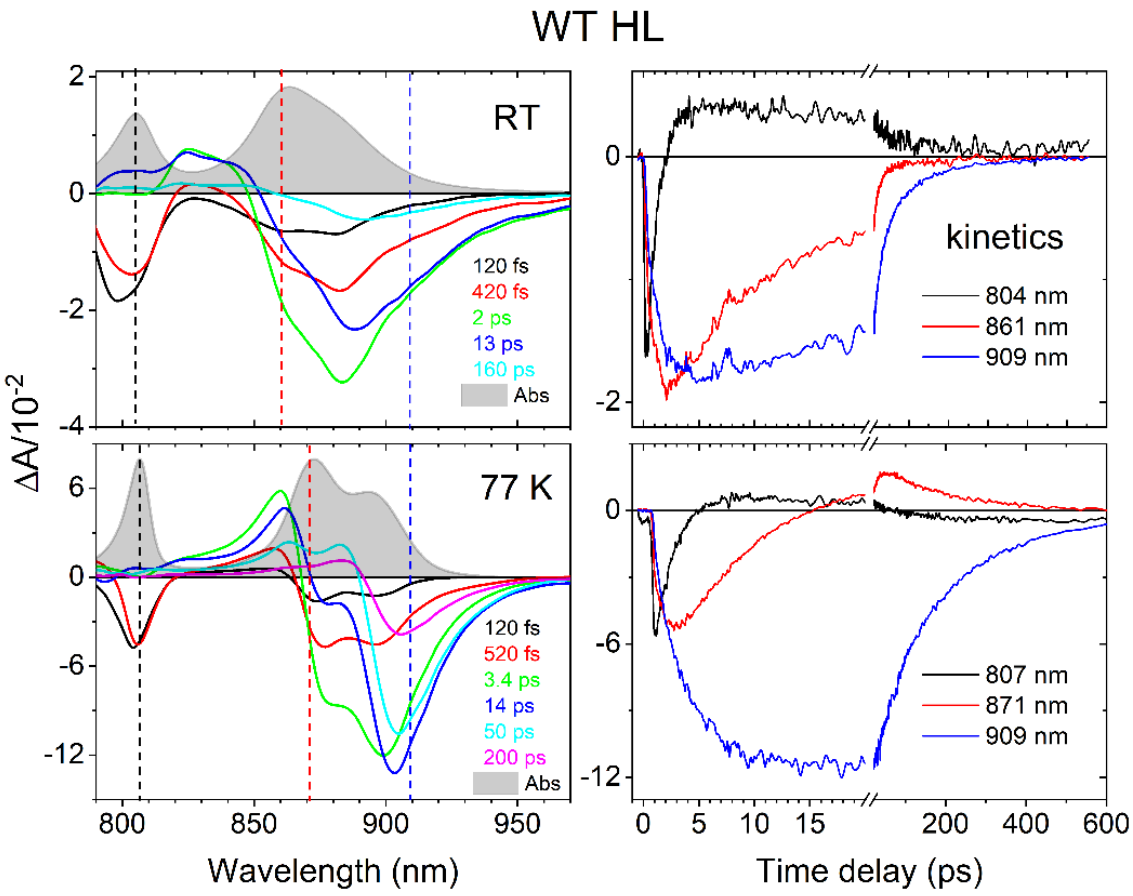

Fig. 4 Transient absorption of the HL ICM from WT *Rps. palustris* taken at RT and at 77 K upon excitation at 800 nm. The left panels show TA spectra taken at various delay times after excitation, overlaid with absorption spectra for comparative purpose. The kinetic traces shown in right panels show absorbance changes (bleaching of absorption and simulated emission) at wavelengths corresponding to the B800 (black), B850 (red) and B875 (blue) bands. The B875 band trace was chosen at wavelength at which steady-state absorption spectrum of LH2 is diminished

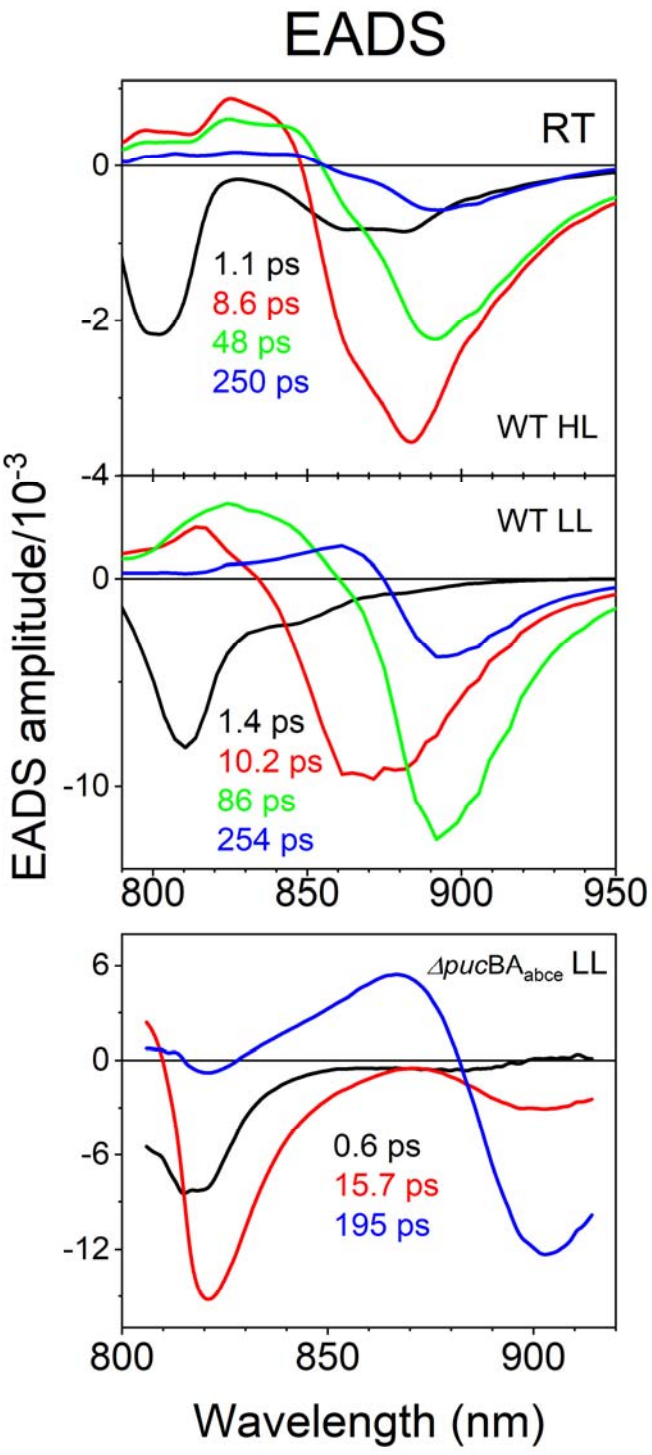

Fig. 5 Global analysis results (EADS) of the TA datasets of ICMs taken at RT (A, C, E) RT.

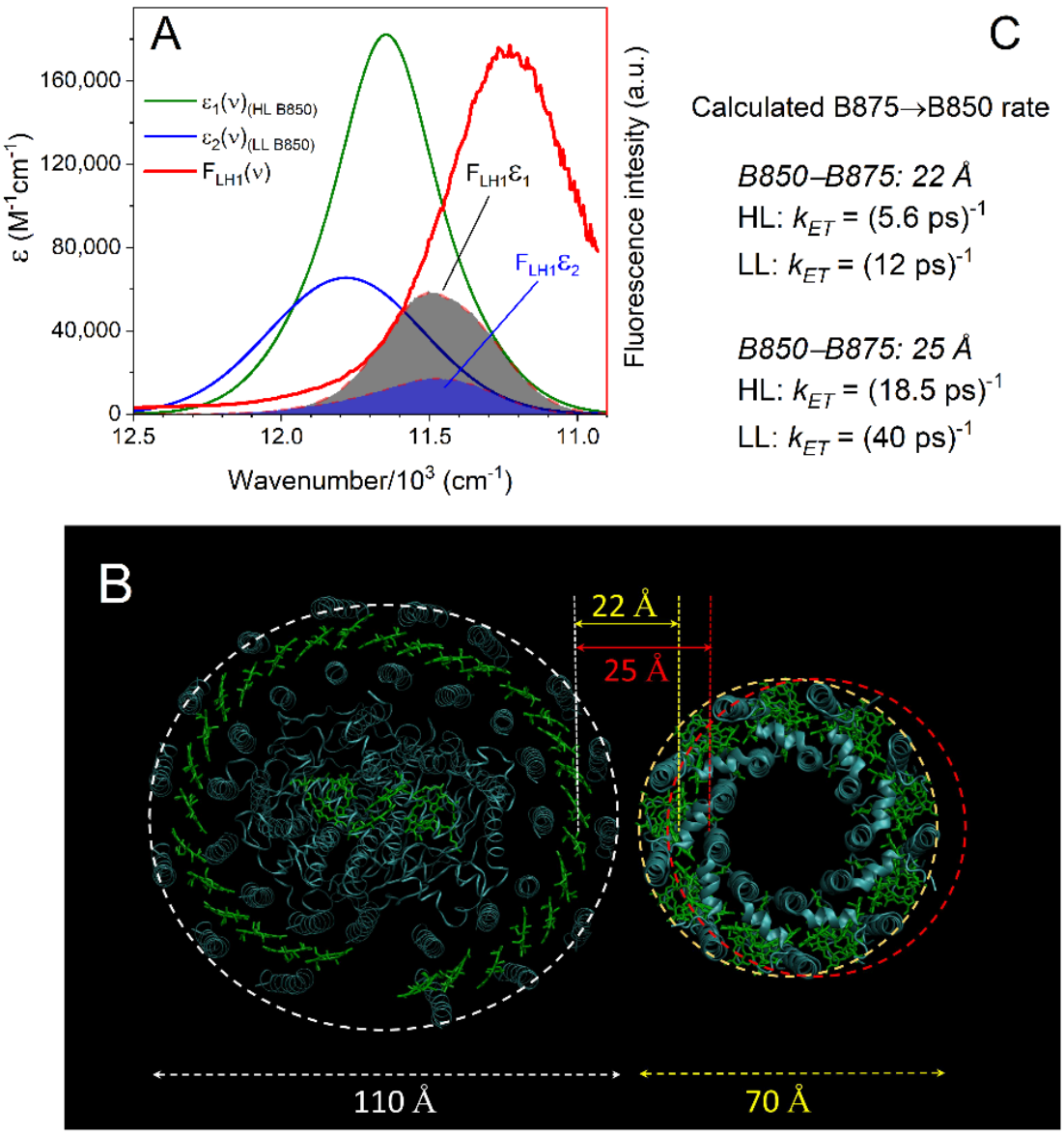

Fig. 6 The LH1→LH2 excitation energy rate modelled with application of Förster resonance mechanism. (A) Molar extinction coefficients of B850 band in LH2 from HL and LL WT ICM overlaid with expected fluorescence emission spectrum of LH1 complex (showed in arbitrary *y* scale) and spectral overlaps. (B) Illustrative sketch of LH1-RC and LH2 complexes in the ICM for two different B875-B850 BChls distances based on 1PYH (Roszak, et al. 2003) and 1KZU (Prince, et al. 1997) crystal structures. (C) Energy transfer rates obtained for two distances between interacting BChls

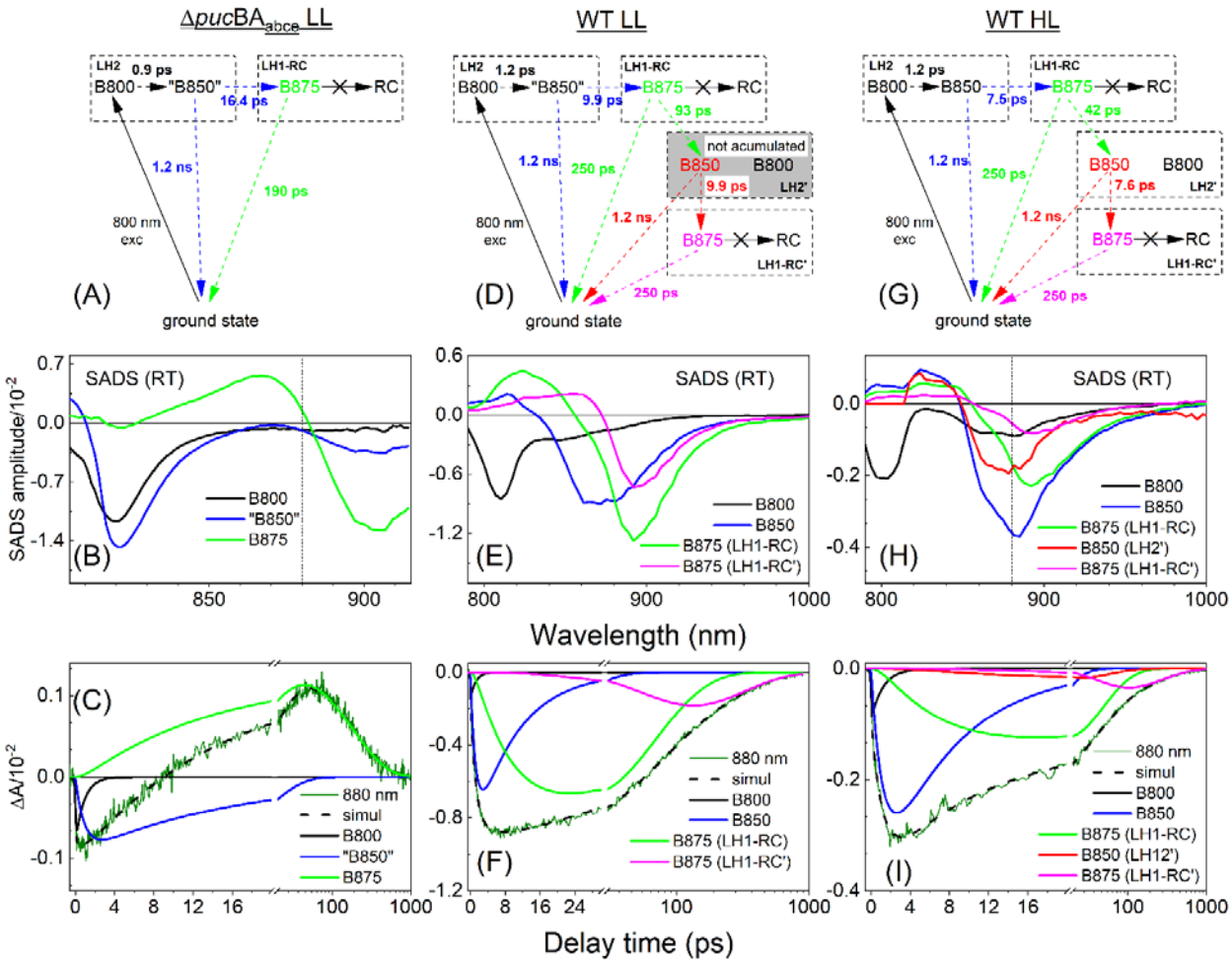

Fig. 7 Kinetic simulation (target analysis) of RT TA datasets of WT HL, LL and Δ*puc*BA$_{abce}$ LL ICMs. (A, D, G) Kinetic models used to simulate datasets, (B, E, H) SADS – spectro-temporal components obtained from simulations. (C, F, I) Exemplary TA traces (880 nm) reconstructed into time-depended contributions of each SADS

References

Aagaard J, and Sistrom WR (1972) Control of synthesis of reaction center bacteriochlorophyll in photosynthetic bacteria. Photochem Photobiol 15:209–225.

Bahatyrova S, Frese RN, Siebert CA, Olsen JD, van der Werf KO, van Grondelle R, Niederman RA, Bullough PA, Otto C, and Hunter CN (2004) The native architecture of a photosynthetic membrane. Nature 430:1058-1062.

Brotosudarmo THP, Collins AM, Gall A, Roszak AW, Gardiner AT, Blankenship RE, and Cogdell RJ (2011) The light intensity under which cells are grown controls the type of peripheral light-harvesting complexes that are assembled in a purple photosynthetic bacterium. Biochem J 440:51-61.

Brotosudarmo THP, Kunz R, Bohm P, Gardiner AT, Moulisova V, Cogdell RJ, and Kohler J (2009) Single-molecule spectroscopy reveals that individual low-light LH2 complexes from *Rhodopseudomonas palustris* 2.1.6. have a heterogeneous polypeptide composition. Biophys J 97:1491-1500.

Carey AM, Hacking K, Picken N, Honkanen S, Kelly S, Niedzwiedzki DM, Blankenship RE, Shimizu Y, Wang-Otomo ZY, and Cogdell RJ (2014) Characterisation of the LH2 spectral variants produced by the photosynthetic purple sulphur bacterium *Allochromatium vinosum*. BBA-Bioenergetics 1837:1849–1860.

Clayton RK, and Clayton BJ (1981) B850 pigment-protein complex of *Rhodopseudomonas sphaeroides* - extinction coefficients, circular-dichroism, and the reversible binding of bacteriochlorophyll. P Natl Acad Sci-Biol 78:5583-5587.

Cogdell RJ, Gall A, and Kohler J (2006) The architecture and function of the light-harvesting apparatus of purple bacteria: from single molecules to in vivo membranes. Q Rev Biophys 39:227-324.

Cogdell RJ, Gardiner AT, Roszak AW, Law CJ, Southall J, and Isaacs NW (2004) Rings, ellipses and horseshoes: how purple bacteria harvest solar energy. Photosynth Res 81:207–214.

Connolly JS, Samuel EB, and Janzen AF (1982) Effects of solvent on the fluorescence properties of bacteriochlorophyll *a*. Photochem Photobiol 36:565–574.

Deinum G, Otte SCM, Gardiner AT, Aartsma TJ, Cogdell RJ, and Amesz J (1991) Antenna organization of *Rhodopseudomonas acidophila* - a study of the excitation migration. Biochim Biophys Acta 1060:125-131.

Dilbeck PL, Tang Q, Mothersole DJ, Martin EC, Hunter CN, Bocian DF, Holten D, and Niedzwiedzki DM (2016) Quenching capabilities of long-chain carotenoids in light harvesting-2 complexes from *Rhodobacter sphaeroides* with an engineered carotenoid synthesis pathway. J Phys Chem B 120:5429–5443.

Dixon JM, Taniguchi M, and Lindsey JS (2005) PhotochemCAD 2: a refined program with accompanying spectral databases for photochemical calculations. Photochem Photobiol 81:212-213.

Evans MB, Hawthornthwaite AM, and Cogdell RJ (1990) Isolation and characterization of the different B800-850 light-harvesting complexes from low-light and high-light grown cells of *Rhodopseudomonas palustris*, strain 2.1.6. Biochim Biophys Acta 1016:71-76.

Fowler GJS, Gardiner AT, Mackenzie RC, Barratt SJ, Simmons AE, Westerhuis WHJ, and Cogdell RJ (1995) Heterologous expression of genes encoding bacterial light-harvesting complexes in *Rhodobacter sphaeroides*. J Biol Chem 270:23875-23882.

Gabrielsen M, Gardiner AT, and Cogdell RJ (2009) Peripheral complexes of purple bacteria. In: Hunter, CN (ed) The purple phototrophic bacteria, Dordrecht; London: Springer

Gardiner AT, Cogdell RJ, and Takaichi S (1993) The effect of growth-conditions on the light-harvesting apparatus in *Rhodopseudomonas acidophila*. Photosynth Res 38:159-167.

Gest H, and Bose SK (1963) Structure and function in bacterial photosynthesis. In: Gest, H, San Pietro, A, and Vernon, LP (ed) Bacterial photosynthesis, Yellow Spring
Ohio: Antioch press, pp. 121-125

Hayashi H, Miyao M, and Morita S (1982a) Absorption and fluorescence spectra of light-harvesting bacteriochlorophyll-protein complexes from *Rhodopseudomonas palustris* in the near-infrared region. J Biochem 91:1017-27.

Hayashi H, Nakano M, and Morita S (1982b) Comparative studies of protein properties and bacteriochlorophyll contents of bacteriochlorophyll-protein complexes from spectrally different types of *Rhodopseudomonas palustris*. J Biochem 92:1805-11.

Herek JL, Fraser NJ, Pullerits T, Martinsson P, Polívka T, Scheer H, Cogdell RJ, and Sundström V (2000) B800 →B850 energy transfer mechanism in bacterial LH2 complexes investigated by B800 pigment exchange. Biophys J 78:2590–2596.

Kiley PJ, and Kaplan S (1987) Cloning, DNA-sequence, and expression of the *Rhodobacter sphaeroides* light-harvesting B800-850-α and B800-850-β genes. J Bacteriol 169:3268-3275.

Koepke J, Hu XC, Muenke C, Schulten K, and Michel H (1996) The crystal structure of the light-harvesting complex II (B800-850) from *Rhodospirillum molischianum*. Structure 4:581-597.

Law CJ, Gardiner AT, Southall J, Roszak AW, Howard TD, Isaacs NW, and Cogdell RJ (2005) How purple bacteria harvest light energy. In: Andrews, DL (ed) Energy Harvesting Materials, Singapore: World Scientific Publishing Co. Pte. Ltd., pp. 65-95

Leblanc HN, and Beatty JT (1993) *Rhodobacter capsulatus* Puc operon - promoter location, transcript sizes and effects of deletions on photosynthetic growth. J Gen Microbiol 139:101-109.

Losev AP, Sagun EI, Kochubeev GA, and Nichiporovich IN (1986) Fluorescence quantum yields, lifetimes, and critical distances for energy transfer for chlorophyll *a* and its pheophytin in solutions. J Appl Spectrosc 45:798-803.

Lüer L, Carey AM, Henry S, Maiuri M, Hacking K, Polli D, Cerullo G, and Cogdell RJ (2015) Elementary energy transfer pathways in *Allochromatium vinosum* photosynthetic membranes. Biophys J 109:1885-1898.

Lüer L, Moulisova V, Henry S, Polli D, Brotosudarmo THP, Hoseinkhani S, Brida D, Lanzani G, Cerullo G, and Cogdell RJ (2012) Tracking energy transfer between light harvesting complex 2 and 1 in photosynthetic membranes grown under high and low illumination. P Natl Acad Sci USA 109:1473-1478.

Ma F, Kimura Y, Zhao XH, Wu YS, Wang P, Fu LM, Wang ZY, and Zhang JP (2008) Excitation dynamics of two spectral forms of the core complexes from photosynthetic bacterium *Thermochromatium tepidum*. Biophys J 95:3349-3357.

Ma YZ, Cogdell RJ, and Gillbro T (1997) Energy transfer and exciton annihilation in the B800-850 antenna complex of the photosynthetic purple bacterium *Rhodopseudomonas acidophil*a (Strain 10050). A femtosecond transient absorption study. J Phys Chem B 101:1087-1095.

Madigan MT (1984) A novel photosynthetic purple bacterium isolated from a Yellowstone hot spring. Science 225:313-315.

McDermott G, Prince SM, Freer AA, Hawthornthwaite-Lawless AM, Papiz MZ, Cogdell RJ, and Isaacs NW (1995) Crystal structure of an integral membrane light-harvesting complex from photosynthetic bacteria. Nature 374:517–521.

Moulisova V, Luer L, Hoseinkhani S, Brotosudarmo THP, Collins AM, Lanzani G, Blankenship RE, and Cogdell RJ (2009) Low light adaptation: Energy transfer processes in different types of light harvesting complexes from *Rhodopseudomonas palustris*. Biophys J 97:3019-3028.

Niedzwiedzki DM, Tronina T, Liu H, Staleva H, Komenda J, Sobotka R, Blankenship RE, and Polivka T (2016) Carotenoid-induced non-photochemical quenching in the cyanobacterial chlorophyll synthase-HliC/D complex. BBA-Bioenegetics 1857:1430–1439.

Paillotin G, Leibl W, Gapinski J, Breton J, and Dobek A (1998) Light gradients in spherical photosynthetic vesicles. Biophys J 75:124-133.

Permentier HP, Neerken S, Overmann J, and Amesz J (2001) A bacteriochlorophyll a antenna complex from purple bacteria absorbing at 963 nm. Biochemistry 40:5573-5578.

Permentier HP, Neerken S, Schmidt KA, Overmann J, and Amesz J (2000) Energy transfer and charge separation in the purple non-sulfur bacterium *Roseospirillum parvum*. BBA-Bioenergetics 1460:338-345.

Prince SM, Papiz MZ, Freer AA, McDermott G, Hawthornthwaite-Lawless AM, Cogdell RJ, and Isaacs NW (1997) Apoprotein structure in the LH2 complex from *Rhodopseudomonas acidophila* strain 10050: modular assembly and protein pigment interactions. J Mol Biol 268:412–23.

Remsen CC (1978) Comparative subcellular architecture of photosynthetic bacteria. In: Clayton, RK and Sistrom, WR (ed) The photosynthetic bacteria, New York: Plenum Press, pp. 31-60

Ritz T, Park S, and Schulten K (2001) Kinetics of excitation migration and trapping in the photosynthetic unit of purple bacteria. J Phys Chem B 105:8259-8267.

Robert B, Cogdell RJ, and van Grondelle R (2003) The light-harvesting system of purple bacteria. In: Green, BR and Parson, WW (ed) Light-harvesting antennas in photosynthesis, Advances in Photosynthesis, Dordrecht, The Netherlands: Kluwer, pp. 169-194

Roszak AW, Howard TD, Southall J, Gardiner AT, Law CJ, Isaacs NW, and Cogdell RJ (2003) Crystal Structure of the RC-LH1 Core Complex from *Rhodopseudomonas palustris*. Science 302:1969–1972.

Sauer K, and Austin LA (1978) Bacteriochlorophyll-Protein complexes from light-harvesting antenna of photosynthetic bacteria. Biochemistry 17:2011-2019.

Scheuring S, Goncalves RP, Prima V, and Sturgis JN (2006) The photosynthetic apparatus of *Rhodopseudomonas palustris*: structures and organization. J Mol Biol 358:83-96.

Scheuring S, and Sturgis JN (2005) Chromatic adaptation of photosynthetic membranes. Science 309:484-7.

Scholes GD, and Fleming GR (2000) On the mechanism of light harvesting in photosynthetic purple bacteria: B800 to B850 energy transfer. J Phys Chem B 104:1854-1868.

Southall J, Henry SL, Gardiner AT, Roszak AW, Mullen W, Carey AM, Kelly SM, de Percin Northumberland CO, and Cogdell RJ (2017) Characterisation of a pucBA deletion mutant from *Rhodopseudomonas palustris* lacking all but the pucBAd genes. Photosynth Res.

Sturgis JN, Tucker JD, Olsen JD, Hunter CN, and Niederman RA (2009) Atomic force microscopy studies of native photosynthetic membranes. Biochemistry 48:3679-3698.

Suzuki H, Hirano Y, Kimura Y, Takaichi S, Kobayashi M, Miki K, and Wang ZY (2007) Purification, characterization and crystallization of the core complex from thermophilic purple sulfur bacterium *Thermochromatium tepidum*. BBA-Bioenergetics 1767:1057-1063.

Tadros MH, Katsiou E, Hoon MA, Yurkova N, and Ramji DP (1993) Cloning of a new antenna gene-cluster and expression analysis of the antenna gene family of *Rhodopseudomonas palustris*. Eur J Biochem 217:867-875.

Tadros MH, and Waterkamp K (1989) Multiple copies of the coding regions for the light-harvesting B800-850 α-polypeptide and β-polypeptide are present in the *Rhodopseudomonas Palustris* Genome. Embo J 8:1303-1308.

van Stokkum IHM, Larsen DS, and van Grondelle R (2004) Global and target analysis of time-resolved spectra. BBA-Bioenergetics 1657:82–104.

Varga AR, and Staehelin LA (1983) Spatial differentiation in photosynthetic and non-photosynthetic membranes of *Rhodopseudomonas palustris*. J Bacteriol 154:1414-1430.

Wu HM, Savikhin S, Reddy NRS, Jankowiak R, Cogdell RJ, Struve WS, and Small GJ (1996) Femtosecond and hole-burning studies of B800's excitation energy relaxation dynamics in the LH2 antenna complex of *Rhodopseudomonas acidophila* (strain 10050). J Phys Chem 100:12022-12033.

Youvan DC, and Ismail S (1985) Light-harvesting-II (B800-B850 complex) structural genes from *Rhodopseudomonas capsulata*. P Natl Acad Sci USA 82:58-62.